Linking the gene regulatory network with the functional physical structure of whole-genome engineered Arabidopsis mutants : an HR-MAS NMR-based metabolomics approach

Augustijn, D.

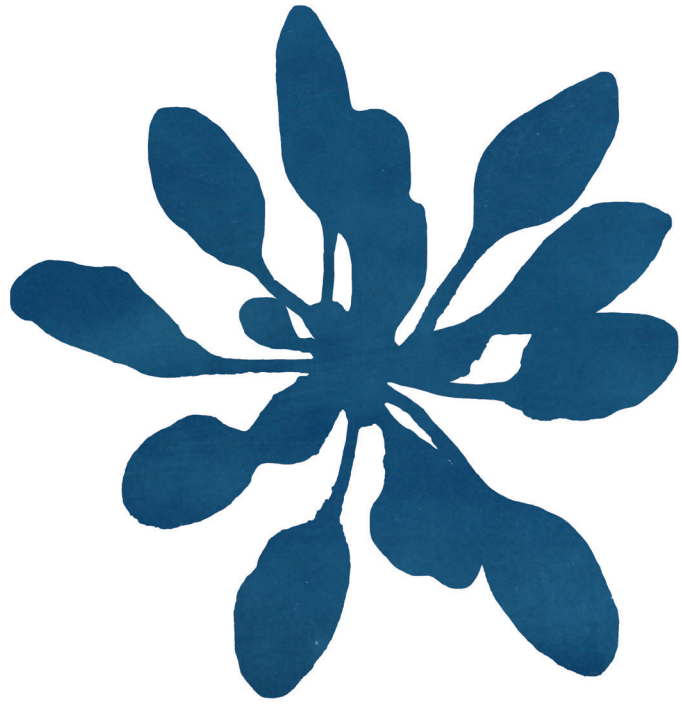

Contrasting metabolite levels and a robust circadian rhythm in *Arabidopsis thaliana* mutants with enhanced growth characteristics

D. Augustijn
N. van Tol
B.J. van der Zaal
H.J.M. de Groot
A. Alia

In preparation

4.1 Abstract

Climate change and the rising food demand provide a need for smart crops that yield more biomass. A genome-wide interrogation approach was used to obtain the *Arabidopsis thaliana* VP16-02-003 and the VP16-05-014 mutants with enhanced growth characteristics by genome-wide reprogramming of gene expression. The photosynthetic machinery is under control of the circadian clock that can perform anticipative switching of the conversion system to prepare plants during the light/dark cycle. We study the metabolic profile at seven different time-points throughout the circadian cycle using high-resolution magic angle spinning (HR-MAS) NMR to investigate the influences of the circadian clock on the metabolic rhythm of the eighteen biomarkers for the larger rosette surface area phenotype. We found that the circadian rhythm of biomarker metabolites is remarkably robust across wild-type Col-0 and VP16-02-003 and the VP16-05-014 mutants, with widely different metabolite levels of both mutants compared to Col-0 throughout the whole circadian cycle. Our analysis reveals that robustness is achieved through functional independence between the circadian clock and primary metabolic processes.

4.2 Introduction

Smart crops with high biomass yield and with a reduced need for fertilizer and pesticides can help to meet the increasing demand for agricultural products.[1,2] Smart crops can be developed by genome editing tools including zinc finger nucleases (ZFNs), transcription activator-like effector nucleases (TALENs) and clustered regularly interspaced short palindromic repeats/Cas9 (CRISPR/Cas9).[3,4] In this study, zinc finger artificial transcription factors (ZF-ATFs) were used to obtain *Arabidopsis thaliana* mutants with enhanced growth characteristics. The transcriptional activator protein VP16 from the herpes simplex virus is fused to an array of three zinc fingers to provide an artificial gene construct, denoted 3F-VP16. Arabidopsis plants are transformed with the 3F-VP16 construct under the control of the promotor of the RPS5α gene. The zinc-fingers can have ±1000 binding sites, both in the coding and in the non-coding DNA of the *Arabidopsis* genome of 130 Mbp. This can lead to drastic changes in genome-wide expression patterns and provide access to rare phenotypes of plants.[4,5] In our previous study, two *Arabidopsis thaliana* mutants, VP16-02-003 and VP16-05-014, with enhanced growth characteristics were obtained using genome interrogation with ZF-ATFs.[6] We have introduced a systems biology approach to resolve primary processes of metabolic regulation and conversion leading to enhanced growth from the complicated biological background.[7]

In the previous work, the metabolic profile for both mutants was studied at one time-point in the middle of the light period of 12 hours in a 24-hour light/dark regime (Chapter 3). The changes in the metabolomics and transcriptomics of both mutants compared to *Arabidopsis* Col-0 gave us insight into the reduced ability to respond to environmental stress of both mutants.[6] Our earlier studies provide converging evidence that the improved growth characteristics of the mutants are a consequence of the reduce defence response in the context of the growth-defence trade-off.[8-10]

It is known that physiological functions, like growth, flowering time, response to stress and metabolism are regulated by the circadian cycle.[11,12] A circadian cycle is a biological

process that displays an endogenous, entrainable oscillation of about 24 hours. Hence the circadian clock comprises three physical entities that fulfil the functional requirements of pre-dawn activation, evening deactivation and the afternoon switching between the morning and evening regimes, providing a nice example of a functional based framework with limited complexity (Figure 4.1A).[13] The molecular mechanism of the circadian clock in *Arabidopsis thaliana* is studied extensively during the last decades and consists of three interlocked transcriptional-translation feedback loops (Figure 4.1B).[11,12,14-16] The central loop of the circadian clock consists of the morning-expressed genes CCA1 (CIRCADIAN CLOCK ASSOCIATED 1) and LHY (LATE ELONGATED HYPOCOTYL) and the evening-expressed gene TOC1 (TIME OF CAB EXPRESSION 1). CCA1 and LHY form a heterodimer which represses the expression of TOC1. The heterodimer also positively regulates the afternoon-expressed pseudo-response regulators PRR5, PRR7 and PRR9. In turn, PRR5, PRR7 and PRR9 repress the transcription of CCA1 and LHY and allows the induction of the evening-expressed gene TOC1. The evening-expressed genes ELF3 (EARLY FLOWERING 3), ELF4 and LUX (LUX ARRYTHMO) will be expressed. These three proteins form the evening complex (EC). The evening complex represses the expression of the PRRs which allows the expression of CCA1 and LHY in the early morning.[11,12,14-16]

According to recent insights into the biological design from a functional perspective, robustness requires functional independence of the abundant subsystems, which, in the case of the clock, are controlled through interfaces while leaving the clock itself undisturbed. I will show this chapter that this is in fact realized in the *Arabidopsis* VP16-02-003 and VP16-05-014 mutants, where gross changes in concentration of primary metabolites are realized while the clock is running the same way across wild-type and mutants.

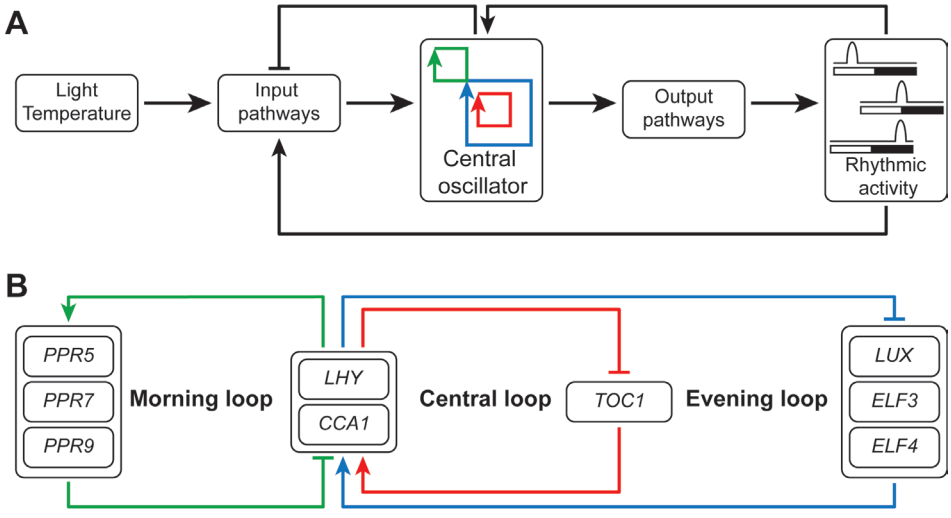

Figure 4.1: Schematic overview of the Arabidopsis circadian clock. A) The central oscillator consists of three interlocked feedback loops. External signals like light and temperature can influence the input pathways for the central oscillator. On his turn, the central oscillator activates output pathways depending on the time of the day. B) Model of the central oscillator containing three interlocked transcriptional-translation feedback loops.

We have studied both the circadian rhythm and the concentration of the metabolites using high-resolution magic angle spinning (HR-MAS) NMR to obtain the metabolic profiles at different time-points of the light/dark cycle for the *Arabidopsis thaliana* wild-type Columbia 0 (Col-0) and two mutants, VP16-02-003 and VP16-05-014. The data provide converging evidence that the clock functional periodicity is independent of mitigation of cellular complexity and growth-defence trade-off.

4.3 Materials & Methods

Plant materials and sample collection

Arabidopsis thaliana plants were grown in soil and cultivated in a climate-controlled growth chamber at 293 K, 70% relative humidity and with a light regime of 12 hours light (200 µmol m^{-2} s^{-1}) and 12 hours dark.[7] The VP16-02-003 and VP16-05-014 mutant with an increased rosette surface area phenotype were investigated in this study in comparison to the wild-type *Arabidopsis* accession Columbia-0 (Col-0).[6] The leaves were harvested at 35 days post germination at seven different time-points throughout the light/dark cycle (Figure 4.2). Samples were frozen immediately in liquid nitrogen and stored at -80˚C.

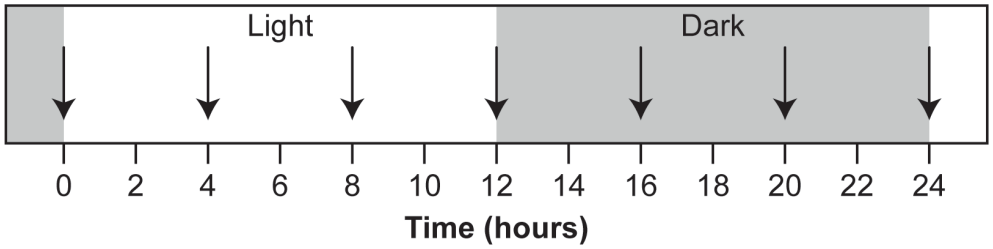

Figure 4.2: Time-points of harvesting of Arabidopsis thaliana Col-0, VP16-02-003 and VP16-05-014 rosette leaves throughout the light/dark cycle.

Quantification of free amino acids, proteins, soluble sugars and starch

The free amino acid content was assayed using the ninhydrin method[17] and the protein content was determined using a Bradford assay.[18] The concentration of soluble sugars was determined using the phenol-sulphuric acid method.[19] The method of Smith and Zeeman was used to determine the starch content of the leaves.[20]

Statistical analysis

The Student's t-test function of OriginPro 2016 software (Northampton, USA) was used to determine the significant differences between Arabidopsis wild-type Col-0, VP16-02-003 and VP16-05-014 for the data for each experiment. Values are presented as means ± standard error (SEM) and statistical significance were determined at $p < 0.05$. The same colours for each class are used throughout the whole chapter.

HR-MAS NMR-based metabolic profiling

A single leaf (n = 6) was inserted into a 4 mm ZrO_2 rotor with 10 µL of deuterated phosphate buffer (100 mM, pH 6) containing 0.1% (w/v) 3-trimethylsilyl-2,2,3,3-tetradeuteropropionic acid (TSP). A Bruker AV-400 MHz spectrometer operating at a resonance frequency of

399.427 MHz was used for the HR-MAS NMR experiments with a 4 mm HR-MAS dual inverse $^{1}H/^{13}C$ probe with magic angle gradient. A spinning frequency of 4 kHz and a temperature of 277 K was used during data acquisition.

A rotor synchronized Carr-Purcell-Meiboom-Gill (CPMG) pulse sequence with water suppression was used to obtain one-dimensional ^{1}H HR-MAS spectra.[21] The one-dimensional spectra were collected applying 256 transients, a spectral width of 8000 Hz, data size of 16K point, an acquisition time of 2 seconds and a relaxation delay of 2 seconds. The free induction decays (FIDs) were exponentially weighted with a line broadening of 1 Hz. TOPSPIN 3.5 (Bruker Analytische Messtechnik, Germany) was used to phase the spectra manually and to perform automatically baseline correction. Gradient-enhanced two-dimensional ^{1}H-^{1}H COSY was obtained to confirm signal assignment.

Multivariate analysis

AMIX (version 3.8.7, BrukerBioSpin) is used to generate bucket tables for each time-point from the one-dimensional spectra excluding the region between 4.20 – 6.00 ppm to remove the larger water signal. The one-dimensional CPMG spectra were normalized to the total intensity and binned into buckets of 0.04 ppm. The data were mean-centred and scaled using the Pareto method in SIMCA software package (version 14.0, Umetrics, Umeå, Sweden). Supervised orthogonal partial least squares discriminant analysis (OPLS-DA) was performed on the data using the SIMCA software.

Quantification of the metabolites

The eighteen metabolites from our earlier metabolomics study of these mutants (Chapter 3) were quantified using the Chenomx NMR Suite 8.2 (Chenomx Inc., Edmonton, Alberta, Canada). The known concentration of the reference peak of TSP was used to determine the concentration of the eighteen biomarkers. Metabolite concentrations are represented as means ± standard error. Student's t-test analysis of the NMR quantification results was performed with OriginPro 2016 (Northampton, USA).

4.4 Results and Discussion

Circadian rhythm of amino acids, proteins, sugars and starch

The functional pathways underlying the enhanced growth characteristics of the VP16-02-003 mutant and the VP16-05-014 mutant were investigated in this study throughout the circadian cycle. Prior to metabolic profiling, the circadian rhythms for the free amino acids, proteins, soluble sugars and starch are assayed (Figure 4.3).

During the dark period, amino acids are degraded.[22] In the wild-type Col-0, the free amino acid concentration shows an increasing trend during the light period and their levels dropped during the night period as expected (Figure 4.3A). Both mutants followed this pattern, and metabolite concentrations in VP16-02-003 were higher than for the Col-0. The concentration of free amino acids for the VP16-05-014 mutant was low at the beginning of the circadian cycle and very similar to the Col-0 in the dark period. The concentration of proteins remains constant throughout the light/dark cycle except for a dip at the beginning of the dark period (Figure 4.3B) and both mutants and wild-type follow the same circadian

rhythm. However, the level of proteins is lower throughout the cycle for the VP16-02-003 and VP16-05-014 mutant relative to Col-0.

In photosynthesis, light drives the assimilation of CO_2 into sugars. These sugars are used for several primary processes in *Arabidopsis thaliana*. Starch can be used in the dark period when light is not available.[23,24] For both sugars and starch, we expect a rhythm where the compound has risen to a maximum at the end of the light period and reduction takes place during the dark period.[23,24] The concentration of sugars in the *Arabidopsis* Col-0 has a peak at 12 hours and reduced during the dark period (Figure 4.3C). The VP16-02-003 mutant follows the same rhythm with a lower concentration throughout the whole cycle. The concentration of soluble sugars is constant for the VP16-05-014 throughout the light/dark cycle. In Col-0, the starch level elevated during the light period and dropped during the dark period (Figure 4.3D). The starch content of the VP16-02-003 mutant was constant during the whole period at a lower level in contrast to Col-0. VP16-05-014 follows the same rhythm as Col-0 but with a lower concentration. Most probably, soluble sugars and starch are not the most favourable carbon storage possibility in these mutants. Organic acids, like fumaric acid and malic acid, can be used as an alternative carbon storage in *Arabidopsis* plants.[25-27] These organic acids have been studied using metabolic profiling as described in the following section.

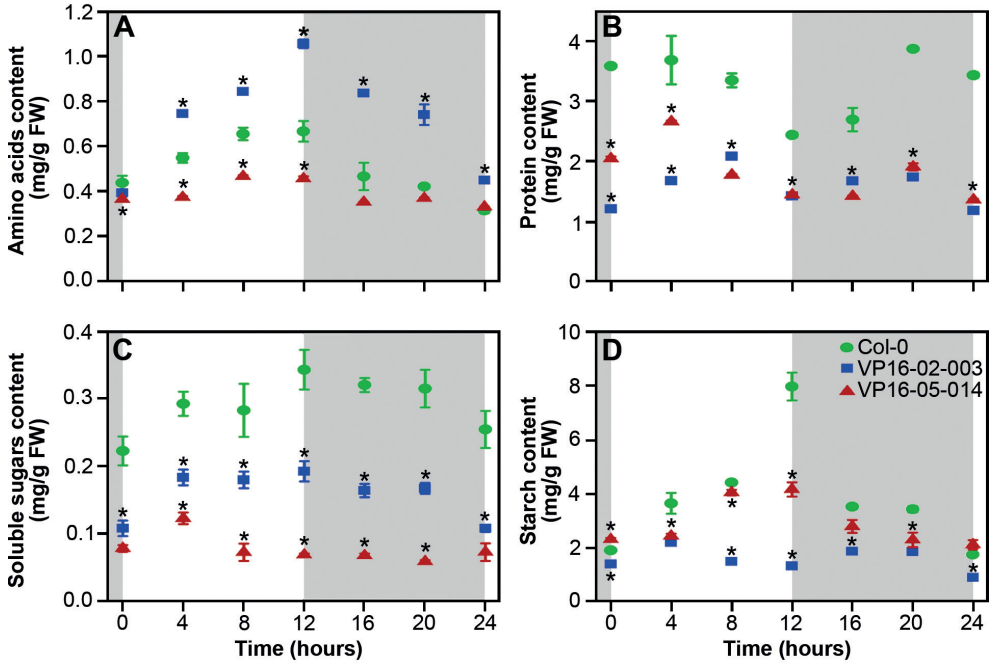

Figure 4.3: Changes in concentration of free amino acids (A), proteins (B), soluble sugars (C) and starch (D) throughout the circadian cycle for Arabidopsis thaliana Col-0 (●), VP16-02-003 (■) and VP16-05-014 (▲) in mg/g fresh weight. The results are given as mean ± SEM. Statistical analysis comparing groups was performed by Student's t-test ($p < 0.05$).*

Metabolic profiling of mutants at different time-points throughout the light/dark cycle using HR-MAS NMR

The metabolic profiles have been obtained from intact leaves of *Arabidopsis thaliana* at different time-points throughout the circadian cycle for the wild-type Col-0 and for both enhanced growth mutants. Figure 4.4 shows representative one-dimensional ^{1}H HR-MAS NMR spectra for Col-0, VP16-02-003 and VP16-05-014 at t = 12 hours.

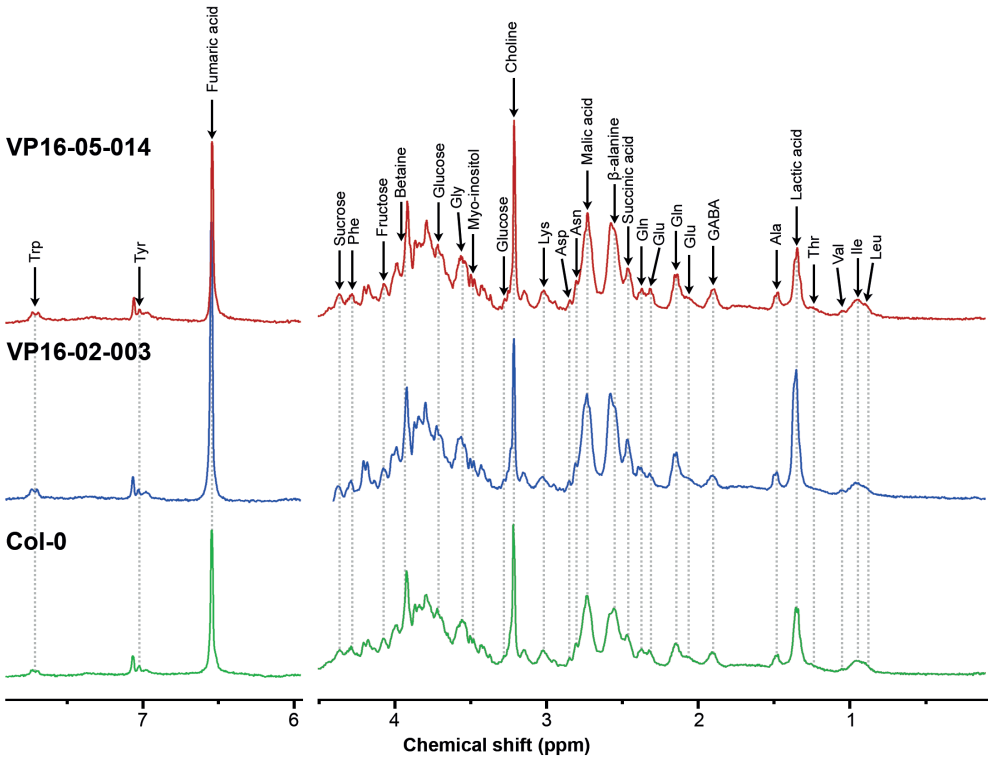

Figure 4.4: One-dimensional ^{1}H CPMG NMR spectra for Arabidopsis thaliana Col-0 (bottom panels), VP16-02-003 (middle panels) and VP16-05-014 (top panels) obtained from intact rosette leaf harvested at t = 12 hours into the light/dark cycle. Main metabolites have been assigned in the spectra.

The metabolic profiles for every time-point obtained by ^{1}H HR-MAS NMR were investigated by multivariate analysis of the bucket-reduced ^{1}H NMR data. Orthogonal partial least square discriminant analysis (OPLS-DA) was carried out to examine the variation in metabolic profile between two mutants and the wild-type Col-0 throughout the light/dark cycle (Figure 4.5). In the OPLS-DA model, this is realized by a separation of the orthogonal and predictive component of the replicates collected from the Col-0, VP16-02-003 and VP16-05-014. The predictive component is correlated with the differences between the Col-0 and mutant classes, while the orthogonal component is uncorrelated with these differences. Hence, in the OPLS-DA score plots, this leads to clustering and separation of the replicates belonging to each class at every time-point of the light/dark cycle.

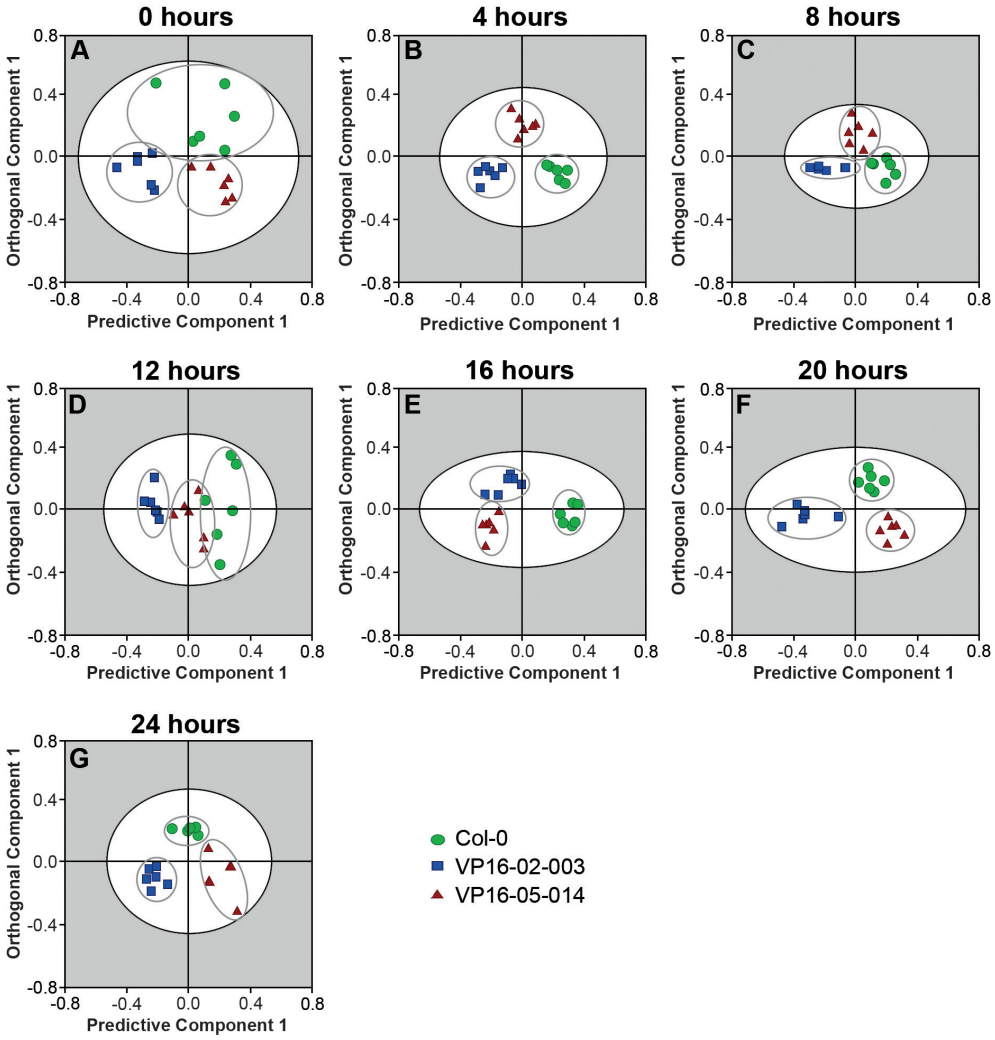

Figure 4.5: Orthogonal partial least square-discriminant analysis (OPLS-DA) score plots of the metabolite profiles derived from the intact leaves of Arabidopsis thaliana wild-type Col-0 (●), VP16-02-003 (■) and VP16-05-014 (▲) at the seven different time-points of harvesting throughout the light/dark cycle (see Figure 4.2).

In an earlier metabolomics study of the VP16-02-003 and VP16-05-014, eighteen biomarkers were identified at t = 6 hours after the start of the light period (Chapter 3). The circadian rhythm of these biomarkers is followed in this study. The primary metabolites that can be observed include the organic acids fumaric acid, malic acid and lactic acid, the sugars fructose and glucose, and the precursor of cell wall components choline (Figure 4.6) and the secondary metabolites myo-inositol, a sugar alcohol, and the organic osmolyte betaine. Also, 10 free amino acids can be resolved with NMR (Figure 4.7).

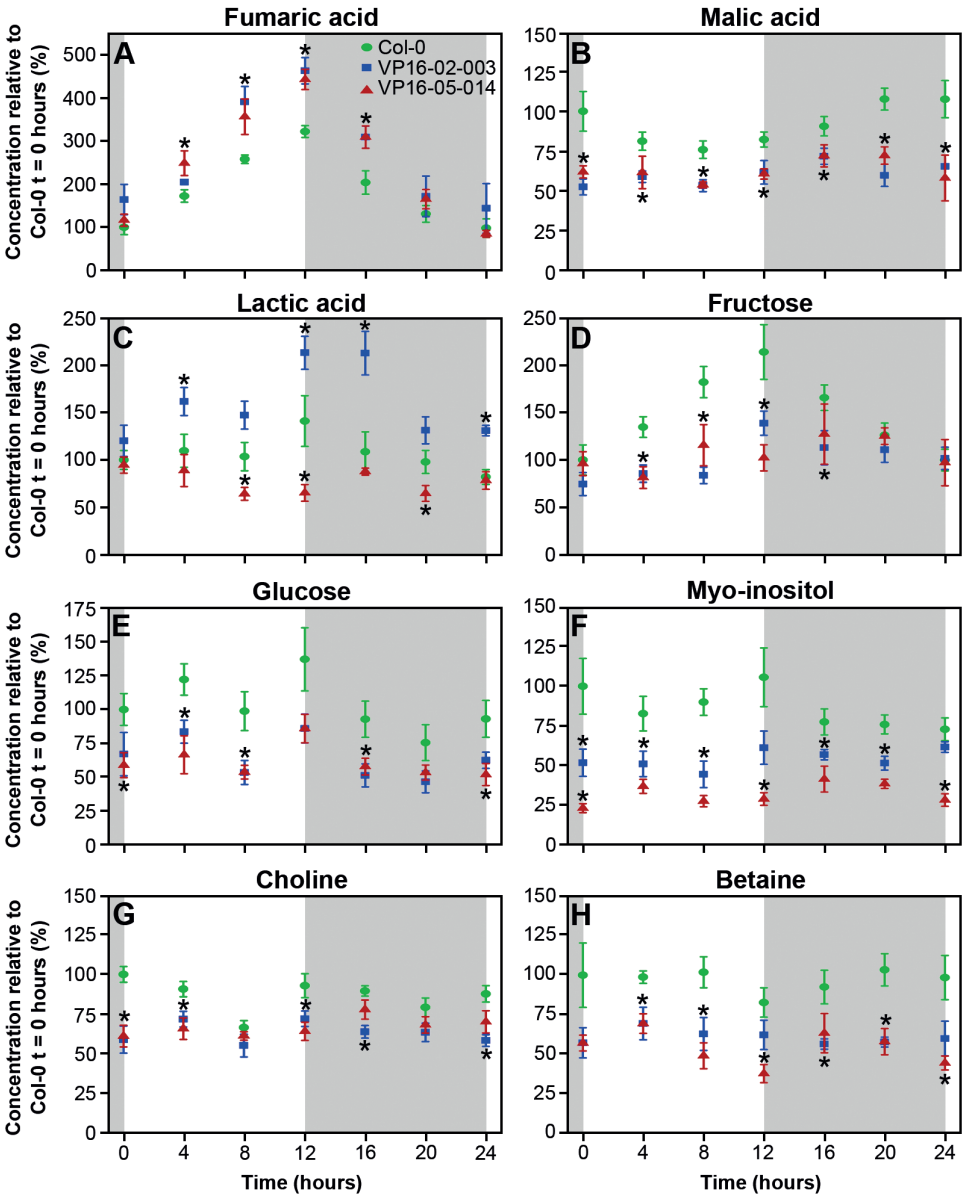

Figure 4.6: Metabolite concentrations during the circadian cycle of fumaric acid (A), malic acid (B), lactic acid (C), fructose (D), glucose (E), myo-inositol (F), choline (G) and betaine (H) in Arabidopsis thaliana Col-0 (●), VP16-02-003 (■) and VP16-05-014 (▲). Means ± SEM of 6 biological replicates is shown. Concentrations are expressed relative to the concentration of Col-0 at t = 0 hours. Statistical analysis comparing groups was performed by Student's t-test ($p < 0.05$). When two data points overlap, an asterisk indicates that both pass the Student's t-test.*

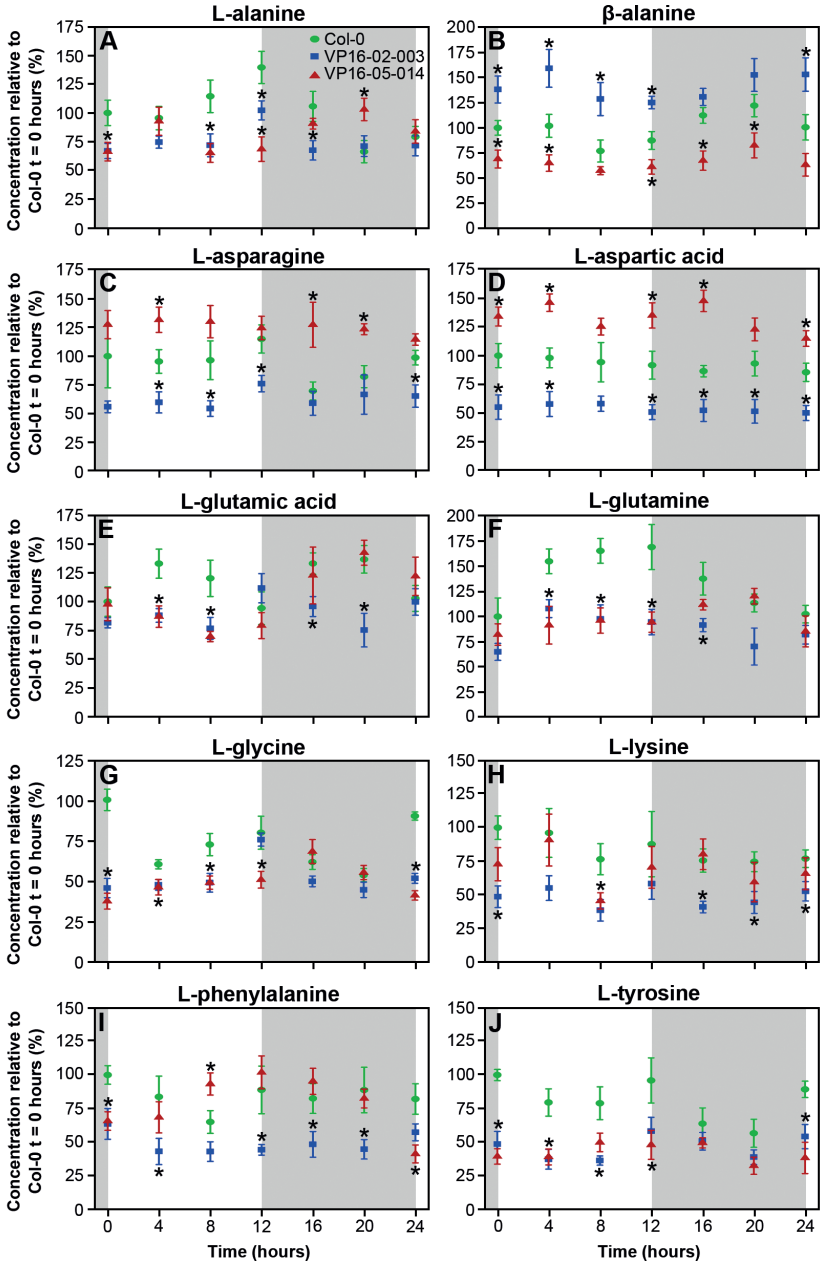

Figure 4.7: Concentration of the free amino acids L-alanine (A), β-alanine (B), L-asparagine (C), L-aspartic acid (D), L-glutamic acid (E), L-glutamine (F), L-glycine (G), L-lysine (H), L-phenylalanine (I) and L-tyrosine (J) throughout the circadian cycle in Arabidopsis thaliana Col-0 (●), VP16-02-003 (■) and VP16-05-014 (▲). Concentrations are expressed relative to the concentration of Col-0 at t = 0 hours. Statistical analysis comparing groups was performed by Student's t-test ($p < 0.05$).*

Characterization of metabolic rhythms throughout the circadian cycle

Fixation of CO_2 during photosynthesis is resulting in different photoassimilates, such as organic acids, sugars and starch. The circadian rhythms of the concentration of the organic acids fumaric acid, malic acid and lactic acid are shown in Figure 4.6A-C. In *Arabidopsis*, fumaric acid is generally considered the major form of fixed carbon and accumulates in the mitochondria and in the cytosol.[26-28] Figure 4.6A and 4.6B show that the concentrations of fumaric acid and malic acid increase during the light to a maximum at the end of the light period and decrease during the dark period in wild-type Col-0 and for both mutants.[7,27] The rhythm of the malic acid concentration in VP16-02-003 and VP16-05-014 remains the same in comparison to the wild-type Col-0, however with a lower concentration. In our earlier study, we found that the concentration of lactic acid is high at the end of the light period and dropped during the dark period in *Arabidopsis thaliana* Col-0.[7] VP16-02-003 follows this rhythm but at a higher concentration, while VP16-05-014 has a lower lactic acid concentration in comparison to Col-0 (Figure 4.6C).

Sugars can also be an intermediate of carbon fixation and play an important role in the circadian rhythms, mainly by regulation of diurnal genes. The photosynthetic carbon fixation during the light period partially produces sugars that can be used during the dark period.[22] Figure 4.6D and 4.6E show the concentration of fructose and glucose during the light/dark cycle. The concentration of fructose and glucose increases during the light period and declines during the dark period in *Arabidopsis* Col-0 and both mutants. VP16-02-003 and VP16-05-014 have lower concentrations throughout the whole light/dark cycle than for the wild-type. Apparently both mutants VP16-02-003 and VP16-05-014 prefer carbon storage into organic acids instead of sugars.

Myo-inositol is synthesized from glucose and has diverse biological roles including phosphate storage, cell wall biogenesis and stress tolerance.[29] Figure 4.6F shows the circadian rhythm of myo-inositol for the wild-type Col-0 and the two mutants VP16-02-003 and VP16-05-014. The variation of the concentration of myo-inositol is very minor over the entire light/dark cycle in Col-0 and the VP16-02-003 and the VP16-05-014 mutant, which is in line with mass spectrometry data collected by Gibon *et al.* for the wild-type.[30] Both mutants have a lower concentration of myo-inositol throughout the whole cycle compared to Col-0.

Choline is an essential metabolite which is needed to synthesize membrane phospholipids in plants. Choline can be oxidized to the organic osmolyte betaine.[31,32] For Col-0, the levels of choline decrease during the light period and increase during the dark period (Figure 4.6G). The VP16-02-003 and VP16-05-014 mutants follow the same rhythm at a lower choline level than for Col-0. The concentration of betaine decreases during the light period and increases during the dark period (Figure 4.6H) in wild-type *Arabidopsis* Col-0, the VP16-02-003 and the VP16-05-014 mutant. The level of betaine is reduced for both mutants compared to Col-0.

Figure 4.7 shows the circadian rhythm of the concentrations of ten free amino acids for the wild-type Col-0 and the VP16-02-003 and VP16-05-014 mutants. The metabolic rhythm of the free amino acids does not differ between the mutants and the wild-type Col-0 (Figure 4.7). The free amino acid alanine, glutamic acid, glutamine, glycine, lysine, phenylalanine

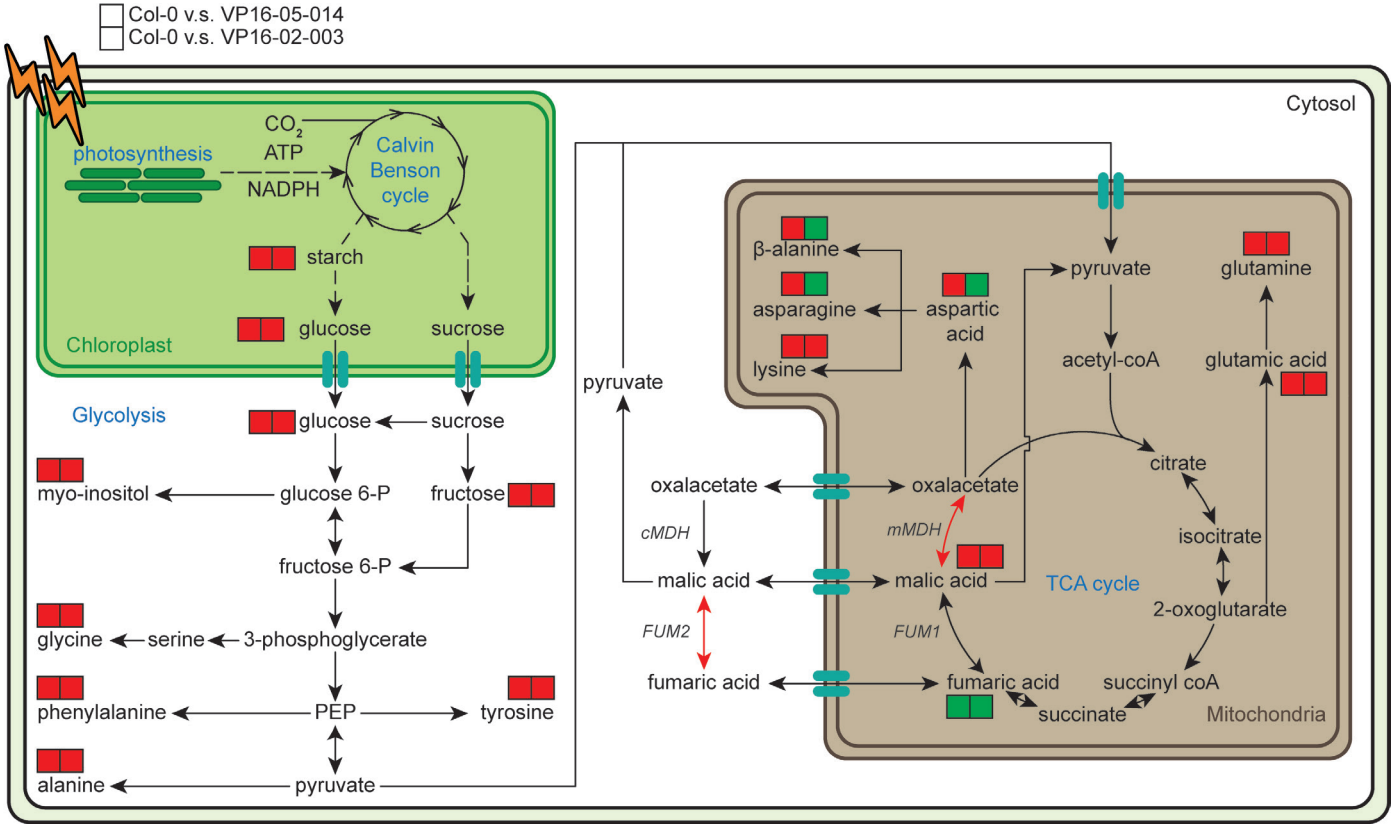

Figure 4.8: Pathway view of the central carbon metabolism of primary metabolites for the VP16-02-003 and VP16-05-014 mutant in comparison to Col-0. Colours indicates higher levels (green) or lower levels (red) of the primary metabolite. Dashed lines indicate multiple conversion steps.

and tyrosine have lower concentrations in both mutants in comparison to Col-0. The concentrations of aspartic acid, asparagine and β-alanine are higher in VP16-02-003 and lower in the VP16-05-014 mutant in comparison to Col-0.

Figure 4.8 summarizes the results of levels of the primary metabolites in comparison to Col-0 in the central carbon metabolism of *Arabidopsis*. What is remarkable is that only the concentration of fumaric acid increases for both mutants relative to Col-0, while the levels of the other primary metabolites are decreased for both mutants. The level of the amino acids aspartic acid, asparagine and β-alanine are upregulated in the VP16-05-014 while these amino acids are downregulated in the VP16-02-003 mutant in comparison to Col-0. Other detected free amino acids have lower concentration for both mutants in contrast to the wild-type. The lower concentrations of sugars, myo-inositol and free amino acids for the mutants compared to Col-0 were attributed to an impaired stress response in the previous chapter 3.

To better understand the high accumulation of fumaric acid, the TCA cycle has been studied in more detail by combining the metabolic data with the mRNA expression levels from the RNA-seq data.[6] The expression level of mitochondrial malate dehydrogenase 1 (mMDH1, AT1G53240) is reduced for both the VP16-02-003 and the VP16-05-014 mutant compared to Col-0. Malic acid can be converted to pyruvate in the mitochondria and in the cytosol. This conversion is facilitated by high concentrations of fumaric acid and may lead to increased fluxes through acetyl-coA back into the TCA cycle.[25]

Fumaric acid and malic acid can be transported to the cytosol and can be interconverted in each other by cytosolic fumarase 2 (FUM2, AT5G50950).[33] The mRNA expression level of FUM2 is reduced for both mutants in comparison to Col-0. The expression level of FUM2 for the VP16-02-003 mutant (logFC = -1.03) is even lower than for the VP16-05-014 mutant (logFC = -0.54). The natural *Arabidopsis* accession Rsch-4 has also reduced expression of FUM2 due to an insertion/deletion polymorphism in the promotor of the FUM2 gene and accumulates high levels of fumaric acid.[33,34] Next to the similarity in high levels of fumaric acid and reduced expression of FUM2, the rosette area of the *Arabidopsis* Rsch-4 is also larger in comparison to Col-0.[35]

The relation between the high levels of fumaric acid and the occurrence of growth vigour is not yet clear. Earlier occurrences of growth vigour in *Arabidopsis* have been related to ploidy and hybridity effects subject to circadian regulation.[36] In addition, epigenetic regulation can lead to growth enhancement.[37] An example is the *Arabidopsis msh1* mutant where the nuclear-encoded MutS HOMOLOGUE 1 (MSH1) gene is downregulated which triggers nuclear epigenetic reprogramming leading to enhanced growth vigour.[37] The zinc finger artificial transcription factors method is a very recent epigenetic reprogramming method to enhance growth.[5,6]

For better understanding, the relation between fumaric acid accumulation and growth vigour, and how primary metabolite concentrations are balanced in the interplay between photosynthetic source and utilization sinks leading to growth, examination of the enzyme activities of malate dehydrogenase and fumarase may lead to underpinning

the underlying mechanisms of conversion of fumaric acid and malic acid.[38] Specific phenotypes can be examined by fluxomics where the metabolic fluxes are studied as the interplay of gene expression, protein concentration, kinetics, regulation and metabolite concentrations.[39] In the general outlook and future outlook (Chapter 5), the fluxomics approach will be described in more detail.

4.5 Conclusion

In this study, we investigated the circadian rhythm of the eighteen earlier identified biomarker for the enhanced growth characteristics phenotype of the VP16-02-003 and VP16-05-014 mutant. HR-MAS NMR was used to obtain the metabolic profile throughout the light/dark cycle for *Arabidopsis thaliana* wild-type Col-0 and the VP16-02-003 and VP16-05-014 mutant. The metabolic rhythm of the eighteen biomarkers is not changed, while the concentrations differ throughout the whole light/dark cycle. Since the clock functional periodicity is independent of the cellular complexity and growth-defence trade-off, the results contribute to converging evidence that it may not be necessary to - upstream - alter the circadian clock when the goal is to achieve enhanced growth characteristics, and that - downstream - phenotypic engineering of sinks and bottlenecks leading to growth may be more effective in a multifactorial context that can be altered by whole genome reprogramming.

4.6 References

[1] C. Mba et al., Agriculture & Food Security 2012, 1, 7–17.
[2] A. Kumar et al., OMICS 2015, 19, 581–601.
[3] V. S. Kamburova et al., International Journal of Agronomy 2017, 2017, 15.
[4] T. Gaj et al., Trends in Biotechnology 2013, 31, 397–405.
[5] N. van Tol, B. J. van der Zaal, Plant Science 2014, 225, 58–67.
[6] N. van Tol et al., PLoS One 2017, 12, e0174236.
[7] D. Augustijn et al., PLoS One 2016, 11, e0163258.
[8] S. Caretto et al., Int. J. Mol. Sci. 2015, 16, 26378–26394.
[9] B. Huot et al., Molecular Plant 2014, 7, 1267–1287.
[10] T. Zust, A. A. Agrawal, Annu Rev Plant Biol 2017, 68, 513–534.
[11] S. Barak et al., Trends in Plant Science 2000, 5, 517–522.
[12] K. Greenham, C. R. McClung, Nat Rev Genet n.d., 16, 598–610.
[13] J. D. Thomas et al., Annu Rev Biophys Biomol Struct 2004, 33, 75–93.
[14] H. Huang, D. A. Nusinow, Trends in Genetics 2016, 32, 674–686.
[15] N. Nakamichi, Plant Cell Physiol 2011, 52, 1709–1718.
[16] J. S. Shim et al., Plant Physiology 2017, 173, 5–15.
[17] S. Gepstein, K. V. Thimann, Plant Physiology 1981, 68, 349–354.
[18] Y. Gibon et al., Plant Cell 2004, 16, 3304–3325.
[19] M. DuBois et al., Anal. Chem. 1956, 28, 350–356.
[20] A. M. Smith, S. C. Zeeman, Nat. Protocols 2006, 1, 1342–1345.
[21] S. Meiboom, D. Gill, Review of Scientific Instruments 1958, 29, 688–691.
[22] O. E. Bläsing et al., Plant Cell 2005, 17, 3257–3281.
[23] M. J. Haydon et al., Nature 2013, 502, 689–692.
[24] M. Seki et al., Sci. Rep. 2017, 7, 8305.
[25] A. U. Igamberdiev, A. T. Eprintsev, Front. Plant Sci. 2016, 7, 513.
[26] M. B. Zell et al., Plant Physiology 2010, 152, 1251–1262.

[27] D. W. Chia et al., Planta 2000, 211, 743–751.
[28] H. Fahnenstich et al., Plant Physiology 2007, 145, 640–652.
[29] P. H. Meng et al., PLoS One 2009, 4, e7364.
[30] Y. Gibon et al., Genome Biol. 2006, 7, R76.
[31] A. Sakamoto, N. Murata, Plant Cell Environ 2002, 25, 163–171.
[32] J. Huang et al., Plant Physiol Biochem 2008, 46, 647–654.
[33] J. Weiszmann et al., 2017, DOI 10.1101/168617.
[34] D. Riewe et al., The Plant Journal 2016, 88, 826–838.
[35] A. Camargo et al., PLoS One 2014, 9, e96889.
[36] M. Miller et al., G3: Genes|Genomes|Genetics 2012, 2, 505–513.
[37] K. S. Virdi et al., Nature Communications n.d., 6, 6386 EP –.
[38] M. Stitt, Y. Gibon, Trends in Plant Science 2014, 19, 256–265.
[39] G. Winter, J. O. Krömer, Environ Microbiol 2013, 15, 1901–1916.